Global and Planetary Change 156 (2017) 59–67

Contents lists available at ScienceDirect

Global and Planetary Change

journal homepage: www.elsevier.com/locate/gloplacha

An aeolian sediment reconstruction of regional wind intensity and links to larger scale climate variability since the last deglaciation from the east coast of southern Africa

M.S. Humphries[a,*], C.R. Benitez-Nelson[b,c], M. Bizimis[b,c], J.M. Finch[d]

[a] Molecular Sciences Institute, School of Chemistry, University of the Witwatersrand, South Africa
[b] Marine Science Program, University of South Carolina, USA
[c] Department of Earth and Ocean Sciences, University of South Carolina, USA
[d] School of Agricultural, Earth and Environmental Sciences, University of KwaZulu-Natal, South Africa

ARTICLE INFO

Keywords:
Aeolian activity
Southern Africa
Westerly winds
Palaeoclimate
LGM

ABSTRACT

Few long-term environmental records are available for southern Africa where shifts in atmospheric circulation and changes in sea surface temperatures interact to influence regional climate dynamics. We present downcore grain size and inorganic geochemistry data covering the last ~23,000 years from a peatland on the east coast of South Africa and examine links between shifts in regional wind activity and palaeoclimatic variability. Our record documents substantial variations in aeolian flux associated with changes in regional climate and wind patterns that reflect larger scale atmospheric circulation patterns. Substantially higher fluxes observed during the Last Glacial Maximum (LGM) are linked to widespread aridification and an expansion in local source areas brought about by a clear shift to dry and cool conditions. Variations in grain size distribution reveal that the aeolian record from Mfabeni comprises two dominant end-members; locally-derived coarse-grained material and a more fine-grained dust component. Marked changes in composition and modal grain size suggest that hydrological shifts in the region during the LGM were accompanied by an increase in storm frequency and wind strength that we link to a northward displacement in the westerly wind belt and a strengthening in wind intensity. Coupling between a rapid increase in sea surface temperature (SST) and an approximate three-fold decrease in aeolian activity after 15 kcal yr BP suggests that changes in SST and its effect on the position and intensity of the westerlies in the Southern Ocean was the dominant climatic driver in the region during deglaciation. Substantially lower aeolian activities through the early Holocene indicate a warming in regional climate and the establishment of more humid conditions under the influence of enhanced tropical easterly flow. Our record also documents more subtle changes in climate over the mid to late Holocene and provides support for an arid phase in southern African climate 6–4 kcal yr BP, as well as an increase in climate variability associated with a strengthening in El Niño–Southern Oscillation (ENSO) activity ~2 kcal yr BP. The study contributes to current knowledge of atmospheric circulation patterns in the Southern Hemisphere and provides new insight into links between aeolian activity, regional wind patterns and climatic variability over glacial-interglacial timescales for a region where existing palaeoclimate records are scarce.

1. Introduction

Changes in the intensity and latitudinal position of the Southern Hemisphere westerly winds since the last deglaciation have been the topic of several recent studies (e.g. Lamy et al., 2010; Marx et al., 2011; Kohfeld et al., 2013). This wind system is widely recognised as an important driver of large scale ocean circulation, regulating global-atmosphere CO_2 exchange, as well as the supply of dissolved nutrients to the Southern Ocean (Anderson et al., 2009; Toggweiler et al., 2006). Changes in the westerly storm tracks have been argued to be a significant factor influencing climate variability in the Southern Hemisphere during glacial-interglacial cycles (Chase and Meadows, 2007; Stager et al., 2012), but although several studies have attempted to reconstruct the position and strength of winds during the Last Glacial Maximum (LGM; 22–18 kcal yr BP) using both terrestrial and marine palaeo-evidence, few continuous records exist (Kohfeld et al., 2013). Limited data from the Southern Hemisphere provides challenges to the development and testing of robust climate models, which are essential

* Corresponding author.
E-mail address: marchump@gmail.com (M.S. Humphries).

http://dx.doi.org/10.1016/j.gloplacha.2017.08.002
Received 17 February 2017; Received in revised form 18 July 2017; Accepted 1 August 2017
Available online 04 August 2017
0921-8181/

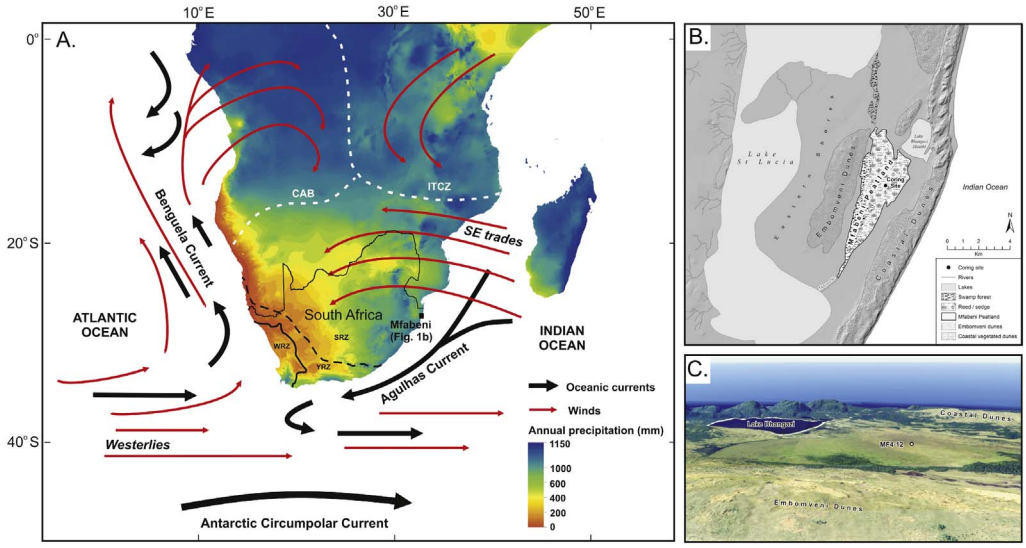

Fig. 1. A) Map of southern Africa showing mean annual precipitation and the present extent of the three major rainfall zones that characterise rainfall variability in the region; winter (WRZ), year-round (YRZ) and summer (SRZ) rainfall zones. The influence of temperate and tropical systems produces a strong west to east rainfall gradient across the subcontinent, from a semi-arid, winter rainfall climate in the west to humid, summer rainfall conditions on the east coast. Major atmospheric and oceanic circulation systems and position of convergence zones (Inter-Tropical Convergence Zone (ITCZ), the Congo Air Boundary (CAB)) are indicated. B) Regional map showing coring location and major local geomorphological features. C) Oblique Google Earth image showing the position of the Mfabeni Peatland and coring location within an interdunal valley (Vertical Exaggeration: 2.5).

for interpreting present and future changes in ocean circulation and nutrient cycles.

Southern Africa occupies a critical position within the Southern Hemisphere for the study of large-scale environmental change over glacial-interglacial cycles. Situated at the interface between tropical and temperate systems, southern Africa's climate is influenced by a variety of major atmospheric and oceanic circulation systems (Fig. 1). Much of southern Africa's long-term climatic variability is thought to reflect changes in the positions of the Antarctic polar vortex, westerly winds, and ITCZ (Tyson, 1999; Stuut et al., 2002). As a result, the subcontinent is well-positioned to examine drivers of climate variability and provide important information on the nature of long-term climate change at both regional and hemispheric scales. However, environmental conditions in southern Africa are typically not conducive to the preservation of palaeoenvironmental archives and records from the region are relatively scarce. Existing records generally cover short timescales, are poorly resolved, and/or are temporally discontinuous (Chase et al., 2015). Moreover, previous studies examining palaeoclimate variability across the subcontinent have generally inferred changes in the position and strength of the westerly winds using indirect proxies of wind conditions, such as from palaeobotanical records (e.g. Chase et al., 2015; Chevalier and Chase, 2015).

Aeolian records from peatlands have been shown to be good indicators of changes in regional storminess and wind patterns (Björck and Clemmensen, 2004; De Jong et al., 2006; Orme et al., 2016), and therefore may provide a more direct proxy for interpreting wind conditions. Mfabeni peatland, on the east coast of South Africa (Fig. 1A), is one of the few terrestrial archives in southern Africa that spans the LGM (Finch and Hill, 2008; Baker et al., 2014). The site occupies an interdunal depression and is therefore in close proximity to an abundant source of material that is susceptible to entrainment during regional storms that reflect larger scale Southern Hemisphere wind patterns (Tyson, 1999). Given the geomorphological setting and lack of fluvial inputs to the study site, the minerogenic content of the peat is considered to reflect material introduced via aeolian processes from both local (e.g., sand dunes) and more distal sources. Changes in the relative proportion and composition of these aeolian components are likely to reflect broader palaeoclimate variations. The Mfabeni peatland therefore provides a unique opportunity to study past changes in wind activity related to intensity and/or positional changes in the westerly winds and large-scale atmospheric circulation over southern Africa.

Here, we present downcore grain size and inorganic geochemistry data covering the last ~23,000 years from the Mfabeni Peatland. We use a combination of grain size, trace element and Sr isotope chemistry to link regional variability observed at the Mfabeni site to larger scale atmospheric circulation patterns and palaeoclimate in southern Africa.

2. Study site

The Mfabeni study area is located on the Maputaland coastal plain in northern KwaZulu-Natal, which is host to the most extensive peat deposits in southern Africa (Ellery et al., 2012). The Maputaland region lies within a sub-tropical climate with hot and humid summers and mild, drier winters. Annual rainfall typically varies between 900 and 1200 mm yr^{-1} and is typically associated with the position of the ITCZ and tropical easterly flow, which transports moisture from the Indian Ocean during the austral summer (Tyson, 1999). The wind regime is characterised by dominant northerly to north-easterly winds during summer, and more intense south-westerly winds during winter that are occasionally associated with storms and frontal depressions brought on by the seasonal intensification and northward expansion of the Southern Hemisphere westerlies winds (Tyson, 1999).

Situated on the eastern shores of Lake St Lucia, the Mfabeni Peatland forms part of the iSimangaliso Wetland Park, a UNESCO World Heritage Site and the largest coastal conservation area in Africa. The peatland lies within an interdunal valley that is bordered to the east by an 80–100 m high Pleistocene-Holocene coastal vegetation dune complex and in the west by the slightly lower (15–70 m), undulating Embomveni dune cordon, which separates the peatland from Lake St. Lucia (Fig. 1B). Dune accretion is linked to a series of marine transgressions and aeolian reworking, and dunes are presently stabilised by a mosaic of coastal forest, woodland, reed swamps and grassland (Porat and Botha, 2008). Peat accumulation began ~55 ka yr ago when the coastal dune separating the peatland from the ocean formed (Porat and Botha, 2008).

Today, Mfabeni extends ~10 km in length (N-S), is ~3 km wide (W-E), covers an area of 1462 ha and contains an ~10 m thick peat sequence at its deepest point (Grundling et al., 2013). Peat accumulation is sustained through local precipitation and persistent groundwater flow emanating from perched aquifers within the coastal sand dunes. There are no fluvial inputs into the peatland and no evidence of previous channel activity since the establishment of the peatland. Minor surface water exchange between Mfabeni and Lake Bhangazi occurs intermittently, driven by local water levels. Peatland vegetation is dominated by herbaceous reed and sedge communities, with swamp forest occurring in the south and along the southwestern margin (Venter, 2003).

3. Methods

3.1. Sample collection and preparation

A series of five continuous sediment cores, ranging from 4 to 7 m, were extracted from the centre of the Mfabeni Peatland during September 2011 and January 2012 using a portable vibracoring system. The coring sites were positioned based on the deepest peat accumulation profiles (Grundling et al., 2000) and where the distance to surrounding dune sand was largest (Fig. 1C). Cores were collected in 72 mm diameter aluminium tubes and transported to the laboratory where they were split longitudinally and described according to the Troels-Smith (1955) sediment classification scheme. In addition, a number of sand samples from the dunes surrounding the site were collected.

The longest (recovery 6.96 m, penetration 8.77 m) of the recovered cores, MF4-12 (28°09′8.1″S; 32°31′9.4″E; 9 m amsl), was subsequently selected for detailed analysis and subsampled at 1-cm intervals. We focus here on the upper section (465 cm) of the profile, representing the period since the LGM. Compaction during coring was corrected based on core recovery (79%) and comparison with previously reported ^{14}C dates from Baker et al. (2014) and Grundling et al. (2013).

3.2. Radiocarbon analyses

Eighteen bulk sediment samples were selected for ^{14}C dating using accelerator mass spectrometry (AMS). Analyses were carried out by Beta Analytic Incorporated, USA and University of Lund, Sweden. Measurements were made on the insoluble residue remaining after standard pre-treatment with HCl and NaOH. Calendar calibrated ages were calculated using the Southern Hemisphere atmospheric curve SHCal13 (Hogg et al., 2013) and Postbomb SH, zone 1–2 (Hua et al., 2013). An age-depth model was derived using the Bacon 2.2 source code within the R statistical environment (Blaauw and Christen, 2011).

3.3. Metal analyses

A total of 44 samples were selected for trace metal analysis based on the age-depth model. Samples dried at 60 °C were weighed, combusted at 500 °C for 4 h, and reweighed to determine loss on ignition (LOI). Combusted sample powders were digested in sub-boiling teflon-distilled HF:HNO_3 mixed acid for two days on a hot plate, dried in concentrated HNO_3 twice and finally diluted with 2% HNO_3 and spiked with 2 ppb In as internal standard. Concentrations were determined at the Center for Elemental Mass Spectrometry at the University of South Carolina using a THERMO ELEMENT2 HR-ICPMS following established techniques in this laboratory for environmental samples (e.g., Das et al., 2013). Low, Medium and High mass resolution modes were chosen to optimize separation of measured isotopes from interfering polyatomics (e.g. ^{75}As from $^{40}Ar^{35}Cl$). Concentrations were determined against an external rock standard (USGS rock standard BHVO-2) and a multi-element standard depending on the signal range of the sample. Internal precision was always better than 5% for all elements. Full procedural blanks were determined along with the samples and were always < 1% of all analytes.

Strontium isotopes were determined on bulk samples using a THERMO NEPTUNE MC-ICPMS, with the PLUS option and an APEX introduction system. Strontium was separated from the matrix in HNO_3 media using the Sr-spec resin (Eichrom, USA). The NBS 987 Sr standard was determined at $^{87}Sr/^{86}Sr = 0.710408 \pm 0.000013$ (2 standard deviations, $n = 7$) and ratios are reported relative to the accepted value of $^{87}Sr/^{86}Sr = 0.710250$. The AGV-2 USGS rock standard was determined at $^{87}Sr/^{86}Sr = 0.704051 \pm 0.000012$ ($n = 4$), within the range reported in the GEOREM database (http://georem.mpch-mainz.gwdg.de/, accessed January 2015). Major elements were analysed by X-ray Fluorescence. Measurements were performed on pressed pellets following calibration against a range of local and USGS rock standards. Concentrations were typically within 10% of accepted values.

3.4. Grain size and mineralogy

Grain size distributions were measured on ash residues, after leaching with 10% HCl to remove carbonates. The resulting well-dispersed sample was analysed using a Malvern Mastersizer 2000 (measuring range: 0.02–2000 μm). A total of 68 samples were processed, with some intervals not yielding sufficient material for analysis. Grain size analyses on dune sand samples were conducted following combustion of the material at 500 °C. Mineralogical investigations were performed using X-ray diffraction on un-orientated powder samples (Bruker D2 Phaser) and scanning electron microscopy (Nova 600 SEM).

3.5. Aeolian sediment influx

The influx of bulk aeolian sediment was calculated as a mass accumulation rate ($g\,m^{-2}\,y^{-1}$) = LSR x DBD x f; where LSR is linear sedimentation rate, DBD is the dry bulk density (determined by water displacement) of the peat, and f is the inorganic proportion (residue remaining after combustion) within the peat. End-member modelling was applied to determine the proportions of distinct sediment components contributing to the measured grain size signal. Volume-size distributions were fitted with log-normal functions based on the parsimony between number of end-members and the goodness-of-fit. Analyses revealed that variations in particle size distributions could be attributed to two distinct populations. In an attempt to isolate and fingerprint the far-travelled wind-borne component, size separation on four bulk samples was performed. Ash residues were suspended in water and left to separate by settling according to Stokes law to yield particles in a size range < 10 μm. This material was then dried and analysed for trace metals and Sr isotopes following the procedures described previously.

4. Results

4.1. Stratigraphy and chronology

The upper 70 cm of the sediment core is very dark brown in colour and highly fibrous, dominated by humus, with presence of herbaceous and fine detritus. From 70 to 465 cm, the core sediments are similarly coloured to the uppermost stratigraphic unit, and relatively homogenous, consisting of smooth amorphous peat, containing humus, with a small proportion of fine detritus and silt.

Eighteen AMS age determinations yielded a coherent age-depth model for the core (Table S1; Fig. 2), indicating a basal age of ~24 kcal yr BP for the 465 cm profile. All age determinations were stratigraphically consistent, with the exception of a single age at 250.5 cm (6.4–6.6 kcal yr BP) which was inverted by 168 years from the upper adjacent age at 183 cm (6.8–7.0 kcal yr BP). This apparent reversal suggests contamination or mixing/bioturbation at this depth. The model designated the age at 250.5 cm as an outlier. Two AMS age determinations at 23 and 30.5 cm, produced results of 103.9 ± 0.3% pMC, and 101.8 ± 0.3% pMC, respectively, indicating that sediments at these depths contained modern (post-1954) carbon.

4.2. Ash content and grain size

Peat inorganic ash contents vary from < 5% to 85% (Fig. 3). Highest ash contents are observed between ~23 and 14.5 kcal yr BP, with values over this period averaging 59 ± 17%. A distinct decrease in ash content is observed at 14.5 kcal yr BP, with the upper section of the core characterised by markedly lower values (averaging 14 ± 7%). Variations in ash content show good correspondence with temporal variations in mean grain size. The coarsest sediments occur

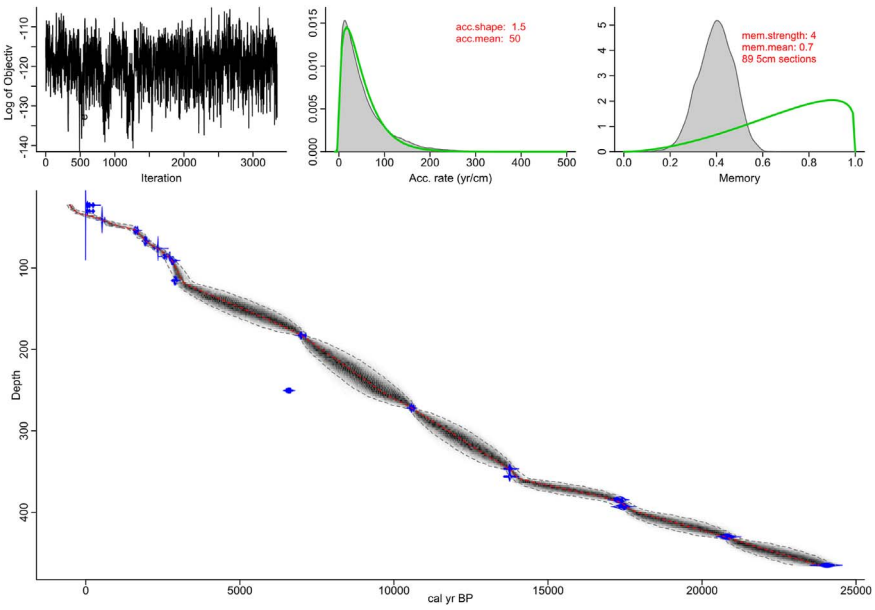

Fig. 2. Mfabeni MF4-12 age-depth model. Calculated in Bacon 2.2 software (Blaauw and Christen, 2011). Calibration performed with southern hemisphere calibration curve, ShCal13 (Hogg et al., 2013) and Postbomb southern hemisphere curve, zone 1–2, for the uppermost modern dates (Hua et al., 2013).

~23–14.5 kcal yr BP and are characterised by a mean grain size of 125 μm. Material deposited after ~14.5 kcal yr BP is distinctly different and generally characterised by markedly finer grain sizes, averaging 50 μm.

In comparison with ice cores, which record mainly atmospheric material transported over a long-range, peatlands also capture aeolian inputs from local and regional sources. Grain size analyses of core material from Mfabeni generally reveal bi-modal distributions that are attributed to the relative contribution of two major end-members (Fig. 4). The two end-members have clearly defined dominant modes, with peaks around 300 μm and 28 μm. The modal size of the coarse end-member is characteristic of local dune sand, while the finer end-member is attributed to dust inputs from more distally located sources. Major variations in grain size distribution through the core can thus be explained by the relative mixing between sand from local dunes and finer material from a more distal source. The relative contribution of each aeolian end-member changes through the record. For example, the coarse-grained component makes up on average ~ 25% of the sediment content of the core between 22 and 18 kcal yr BP, but is relatively low (averaging 13%) in samples from 15 kcal yr BP to present.

4.3. Chemical composition

Material deposited between 22 and 18 kcal yr BP shows significant enrichment in Ti, typically 3–6 times relative to upper continental crust (UCC) values (Fig. 3). Strong correlation between Ti and Nb (R^2 = 0.95) abundances (Fig. S1) suggests that these metals are largely controlled by a Ti-rich heavy mineral phase, which XRD and SEM analyses indicate is ilmenite. From ~14.5 kcal yr BP, Ti abundances approach typical crustal values before increasing again between ~7

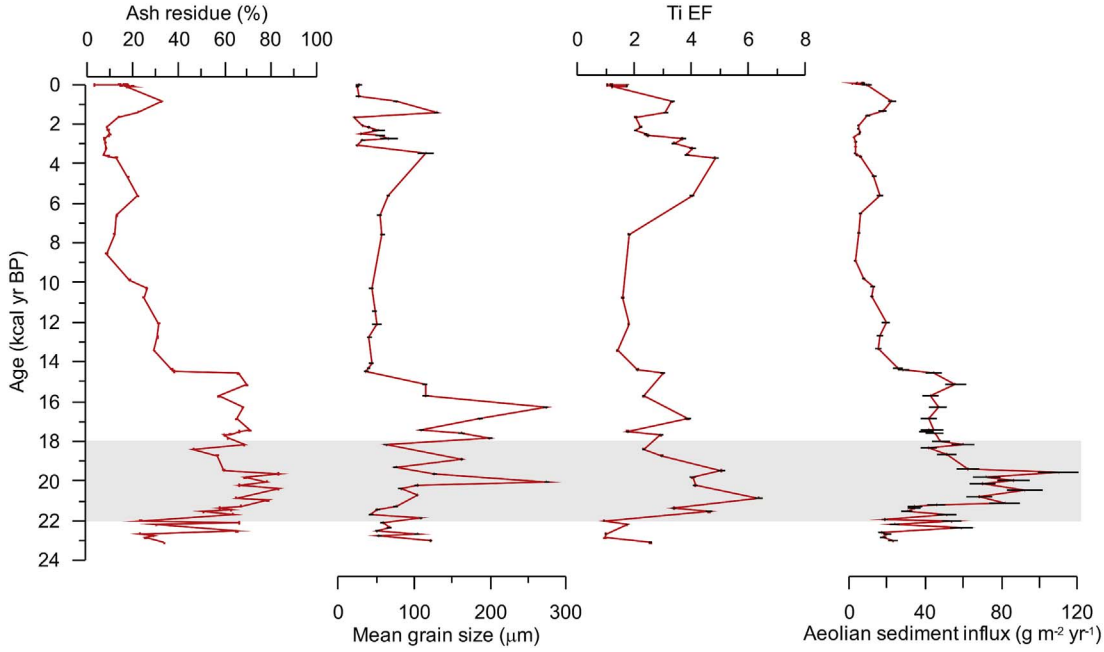

Fig. 3. Variation in peat ash content, mean grain size, geochemistry and calculated aeolian sediment influx. Crustal enrichment factor (EF) for Ti (EF = $(Ti/Sc)_{sample}$ / $(Ti/Sc)_{crust}$) calculated using upper continental crust (UCC) values from Wedepohl (1995). Error bars are compounded and reflect the standard deviation of multiple measurements of Ti and Sc. LGM highlighted by grey box.

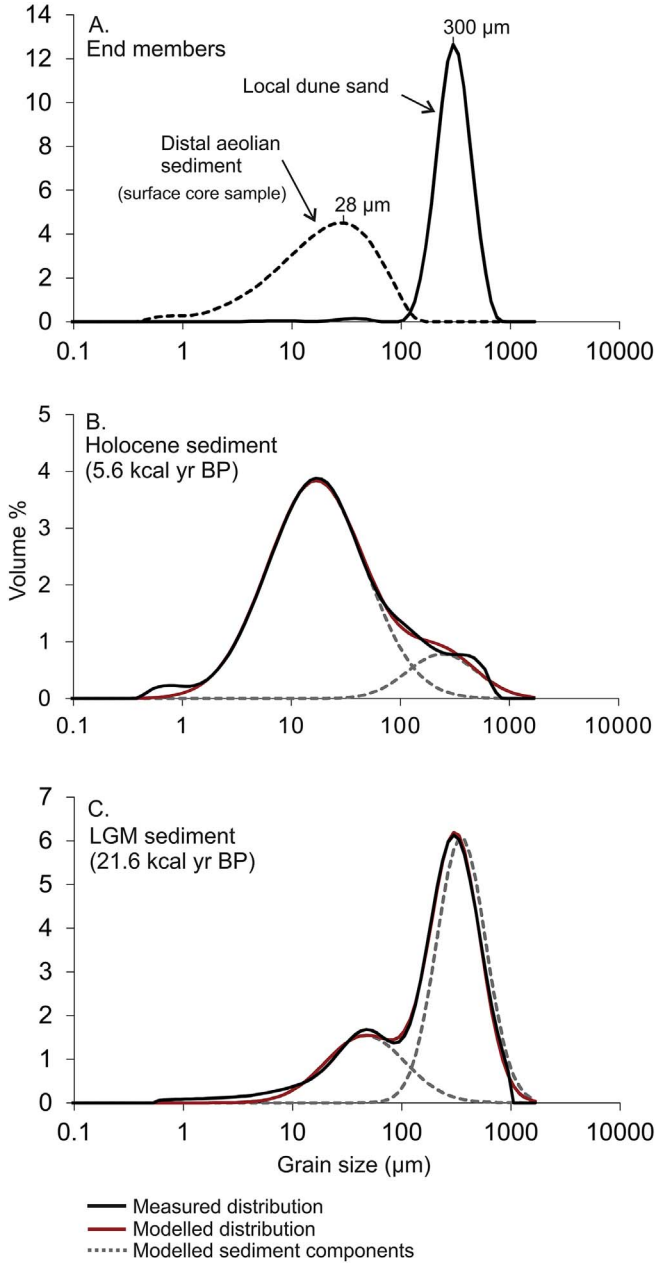

Fig. 4. Selected representative grain size distributions showing the identified aeolian end-members; local dune sand (mode = 300 μm) and a more fine-grained dust component (mode = 28 μm). Fitted log-normal distributions indicate that the presence of bimodal grain size distributions in core samples is consistent with the mixing of these two major end-members. The boundary between the two end-members occurs at ~110 μm.

and 3 kcal yr BP, concomitant with an increase in grain size.

Trace element data support grain size analyses and suggest that material deposited in Mfabeni is composed of two distinct components; a coarse, locally-derived fraction dominated by quartz and high Ti concentrations (e.g., dune sand) and a clay-silt fraction that displays trace element enrichment and is representative of more far-travelled material (Fig. 5). Grain size and trace element abundances indicate that the dunes surrounding the study site are an important source of local aeolian material. The dunes are mineralogically simple, consisting largely (> 99%) of quartz with minor amounts of ilmenite (the source of Ti) and zircon. The transport and deposition of local dune sand into the peatland thus has the net effect of diluting the trace element content of more far-travelled aeolian components, and can therefore be used to interpret changes in storminess and/or wind intensity.

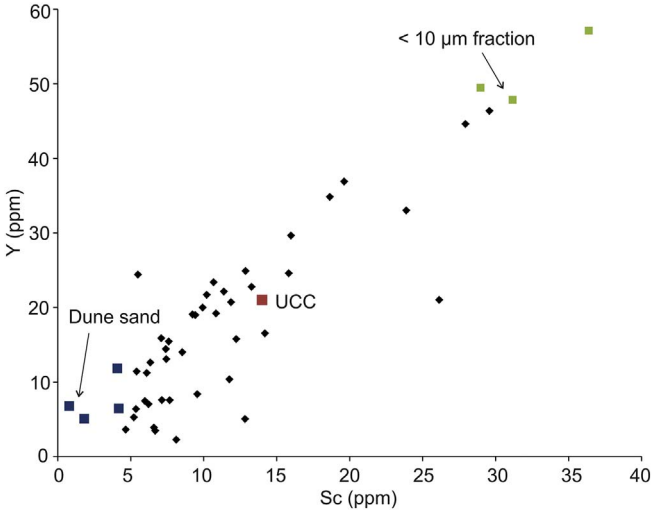

Fig. 5. Variation in Y and Sc abundances within peat ash samples. Y and Sc are largely immobile during diagenesis and present in low concentrations in seawater, and therefore represent tracers of minerogenic inputs. The composition of samples represents the relative mixing between dune sand and a fine-grained component. Upper continental crust (UCC) falls in between these two populations.

In contrast, elements such as Sr and Ba are decoupled from other trace elements, requiring an additional component to the mixing of local and distal aeolian sources. Sr/Sc ratios increase significantly from approximately crustal values (13 − 22) between 23 and 6 kcal yr BP, to > 120 over the last 4 kcal yr BP (Fig. S2). Ba/Sc ratios show a similar trend and generally correlate with an increase in Ca/Sc ratios. Increases in both Ba and Sr over the last 4 kcal yr BP are consistent with SEM analyses, which revealed the presence of carbonate and gypsum within the peat.

Strontium isotope ratios also appear to correlate with shifts in Sr and Ba enrichments. Material from ~21–14.6 kyr is characterised by bulk $^{87}Sr/^{86}Sr$ ratios in the range of 0.715–0.717 (Table 1), typical of continental crustal material. In contrast, the Sr isotopic composition of samples analysed from the last 4 kyr is significantly less radiogenic ($^{87}Sr/^{86}Sr$ = 0.711–0.712) and closer to the composition of seawater ($^{87}Sr/^{86}Sr$ = ~0.708). The Sr isotopic composition of the < 10 μm fraction broadly reflects the same temporal trends, although samples analysed from the ~21–19 cal yr BP period are distinctly less

Table 1
Strontium isotopic data.

Sample	Age (cal kyr BP)	$^{87}Sr/^{86}Sr$ (± 2σ × 10^{-6})
Bulk material		
MF4_1	0.011	0.711782 (± 9)
MF4_2	0.042	0.711535 (± 7)
MF4_3	1.6	0.711090 (± 10)
MF4_4	2.3	0.710949 (± 8)
MF4_5	3.0	0.710939 (± 7)
MF4_6	3.2	0.710972 (± 9)
MF4_7	3.7	0.711478 (± 10)
MF4_8	10.7	0.713629 (± 12)
MF4_9	14.6	0.716183 (± 10)
MF4_10	17.7	0.715066 (± 10)
MF4_11	18.6	0.715139 (± 5)
MF4_12	19.3	0.716618 (± 9)
MF4_13	20.0	0.715818 (± 9)
MF4_14	21.2	0.714939 (± 7)
< 10 μm fraction		
MF4_2f	0.042	0.711663 (± 7)
MF4_12f	19.3	0.713314 (± 1)
MF4_13f	20.0	0.713615 (± 5)
MF4_14f	21.2	0.712535 (± 4)

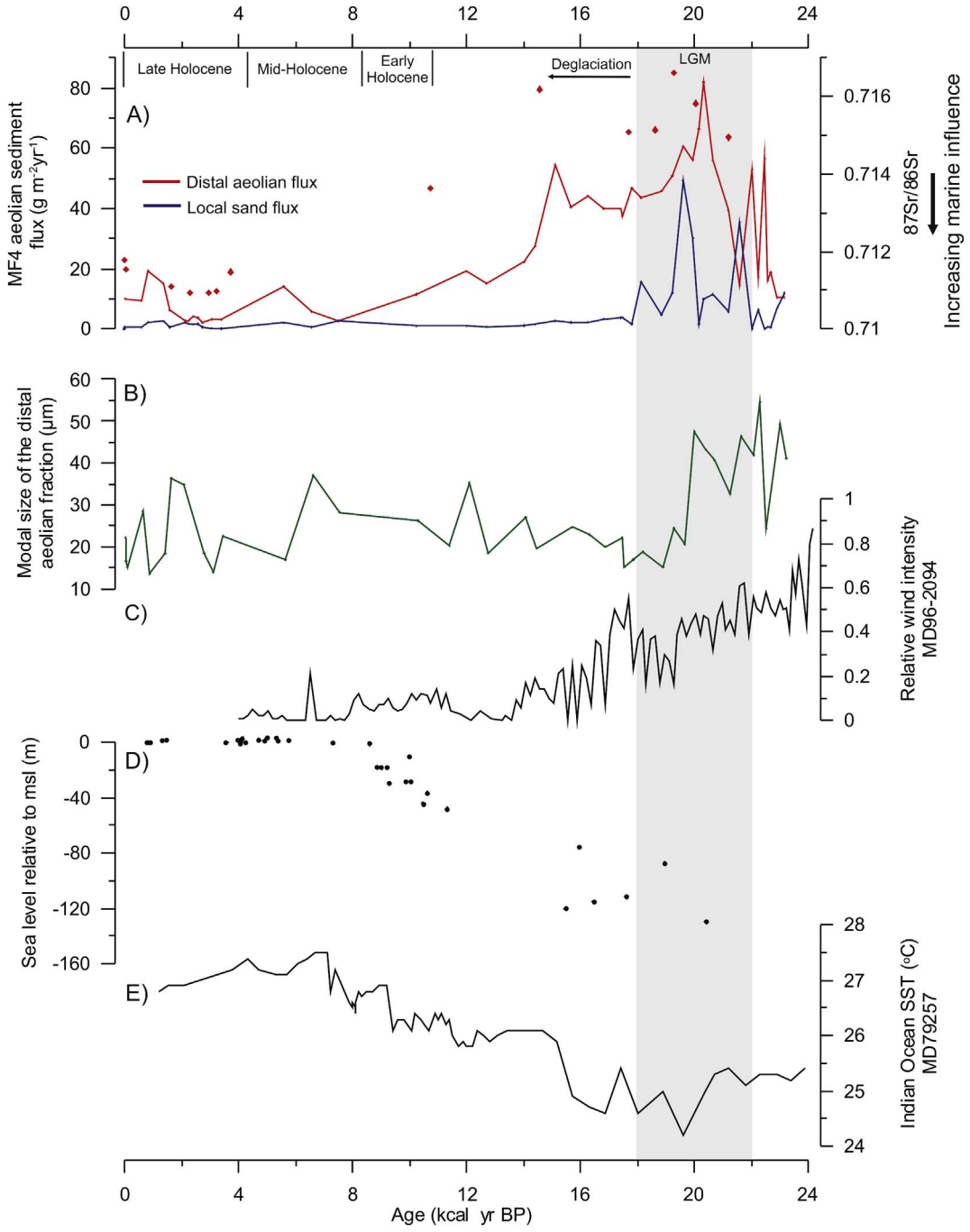

Fig. 6. Comparison between major marine and terrestrial palaeoenvironmental archives from southern Africa. A) Aeolian sediment flux reconstruction from Mfabeni (this study) showing the contribution of distal (dust) and locally-derived (dune sand) material. $^{87}Sr/^{86}Sr$ composition indicated as red diamonds; B) Variation in the modal size of the distal aeolian component; C. Grain size-inferred SE trade wind strength intensity (Stuut et al., 2002); D) Relative sea level based on available indicators from the South African coast and shelf (Ramsay and Cooper, 2002; dates calibrated using SHCal13); E) Alkenone-inferred sea surface temperature (SST) from marine core MD79–257 (Bard et al., 1997). (For interpretation of the references to colour in this figure legend, the reader is referred to the web version of this article.)

radiogenic than their corresponding bulk samples (Table 1). The shift in Sr isotopes toward less radiogenic values corresponds well with an increase in sea level (Fig. 6), which would make marine-derived Sr more readily available to the local environment. The decoupling of Sr concentrations and Sr isotopes therefore likely reflects a distinctly local character in the Sr signal that is superimposed on the overall change in aeolian sources.

4.4. Aeolian sediment fluxes

Calculated bulk aeolian fluxes reveal a number of notable periods of enhanced aeolian deposition (Fig. 3), with highest rates (up to 100 g m^{-2} yr^{-1}) recorded between 22 and 18 kcal yr BP. Fluxes decrease dramatically by a factor of two at ~19 kcal yr BP and average 47 ± 6 g m^{-2} yr^{-1} until 15 kcal yr BP. The period from 15 kcal to present is characterised by even lower fluxes, with values averaging 7.8 ± 5 g m^{-2} yr^{-1}. A modest increase in aeolian flux occurs at 7–4 kcal yr BP and 2–0.9 kcal yr BP, before declining toward present-day levels (6.5 ± 3 g m^{-2} yr^{-1}).

The results of end-member modelling indicate that the relative contribution of local sand and dust to the total aeolian flux varies through the record (Fig. 6A). Overall, the contribution of local sand to

calculated total fluxes is relatively low ($< 2\ g\ m^{-2}\ yr^{-1}$), but increases substantially between 22 and 18 kcal yr BP. Although highly variable over this period, local sand fluxes increase up to $49\ g\ m^{-2}\ yr^{-1}$, accounting for ~45% of the total aeolian flux. Variations in the proportion of the local sand component are accompanied by a shift in the modal grain size of the dust component (Fig. 6B). Highest values are observed during the LGM, with modal grain sizes frequently exceeding 40 μm. A shift to substantially smaller diameters occurs after ~19 kyr BP, with modal values averaging 25 μm during the Holocene.

5. Discussion

5.1. Variability in aeolian sand influx

The presence of extensive sand dune complexes on the Maputaland coastal plain provides a potentially significant local source of easily erodible coarse-grained (125–500 μm) material that can be used to track regional climate change and linked to broader scale climate variability. Substantial variations in aeolian activity through the Mfabeni record point to changes in sediment availability linked to source area and wind climate.

The LGM marks the period of highest aeolian activity in our record, with fluxes ~8 times higher than the average recorded over the Holocene ($7.8 \pm 5\ g\ m^{-2}\ yr^{-1}$) and 14 times higher than present day levels ($6.5 \pm 3\ g\ m^{-2}\ yr^{-1}$). Enhanced aeolian fluxes are interpreted to reflect regional aridity accompanied by the creation and expansion of source areas. The Mfabeni record thus provides evidence for regionally dry and cool climatic conditions that favoured sparser vegetation cover and the mobilization of greater quantities of aeolian material during the LGM. This is supported by pollen records from Mfabeni, which suggest that communities dominated by dry grassland persisted during this time (Finch and Hill, 2008). Geochemical and grain size analyses indicate that local dunes were an important source of material during the LGM. The deposition of quartz-rich material ranging between 125 and 500 μm in size indicates that higher fluxes during this period were driven, in part, by increased input of local dune material.

While increases in aeolian flux can be related to increases in aridity and the expansion of source areas, variations in the modal diameter of particles can be used to infer changes in wind intensity. In our record, an increase in the modal grain size of dust deposited during the LGM suggests enhanced wind transport during this period. Higher wind speeds should transport heavier particles and we also observe increases in Ti concentrations at the LGM. We therefore infer that regionally cool, dry conditions persisted during the LGM and were accompanied by a strengthening in wind climate,

In our core, evidence for the last deglaciation is seen after ~15 kcal yr BP, reflected by sharp declines in aeolian flux, modal grain size and Ti concentrations (Figs. 3, 6). A shift in bulk $^{87}Sr/^{86}Sr$ ratios toward relatively less radiogenic values over the glacial-interglacial transition suggest an increased marine influence consistent with increases in regional sea surface temperature (SST) (Fig. 6E) and higher sea levels (Fig. 6D), with the transport of sea spray possibly aided by an increased dominance in onshore easterly winds. Collectively, this evidence points to a warming in regional climate and greater precipitation that supported dune stabilisation, most likely through increased vegetation cover. An increase in sea level also likely raised groundwater tables and initiated the formation of interdune wetlands, thus impeding deflation. A marked decrease in local sand fluxes and lower Ti concentrations over this period also point to a weakening in dune deposition.

Termination of the LGM through to the mid-Holocene is marked by decreased aeolian sedimentation that we link to warmer and more humid conditions, characterised by increased vegetation cover inhibiting significant regional sediment entrainment. Suppressed aeolian fluxes through the mid and late Holocene are interrupted by two events at 6–4 kcal yr BP and 2–0.9 kcal y BP (Fig. 6A). Higher aeolian fluxes during these periods are coupled with increases in both grain size and Ti concentration, and reflect the input of regional dune material into the peatland under drier and possibly more variable climatic conditions.

5.2. Palaeoclimate interpretation

5.2.1. LGM (22–18 kcal yr BP)

The aeolian record from Mfabeni shows evidence of major global and regional climate events known to have affected southern Africa. Highest rates of aeolian sedimentation in our record are coincident with the LGM, a period of increased aridity across much of southern Africa (Chase and Meadows, 2007; Truc et al., 2013; Chevalier and Chase, 2015). In our record, enhanced aeolian activity coupled with radiogenic $^{87}Sr/^{86}Sr$ signatures provide evidence for regionally dry and cool climatic conditions during the LGM, which reduced vegetation cover, increased source area and resulted in the mobilization of greater quantities of aeolian material. Locally, this is substantiated by OSL dates obtained from the dune cordons (Porat and Botha, 2008), which suggest that environmental conditions across the coastal plain were conducive to widespread dune mobility during MIS2 (29–14 ka). Pollen data from Mfabeni (Finch and Hill, 2008) also support regionally cooler and drier conditions centered at ~21 kcal yr BP, with a quantitative reconstruction of mean annual temperature based on this pollen sequence indicating a 2 °C depression at Mfabeni over the LGM (Chevalier and Chase, 2015). Although limited information regarding the LGM is available for southern Africa, our aeolian record is consistent with other regional palaeoclimate records (Holmgren et al., 2003; Truc et al., 2013) that indicate widespread cooling and desiccation, as well as with temperature and dust records from Antarctica that show elevated dust fluxes during the LGM (Mahowald et al., 1999; Lambert et al., 2012; Kohfeld et al., 2013).

In southern Africa, overall colder and drier conditions during the LGM have been attributed to the expansion of Antarctic sea-ice and its impact on the latitudinal position of the oceanic and atmospheric fronts in the Southern Ocean (Tyson, 1999; Holmgren et al., 2003; Chase et al., 2013). During glacial periods, the mid-latitude westerly winds migrate equatorward and extend further across the subcontinent. Reduced influence of tropical easterly flow results in lower annual precipitation in the summer rainfall region of South Africa (Chase and Meadows, 2007). Although links between climate variability and the position of the westerlies are supported by similar findings from Australia, Chile and New Zealand (e.g., Hesse and McTainsh, 1999; Lamy et al., 2010; Marx et al., 2011), there is less agreement regarding possible changes in wind intensity. A shift toward coarser modal grain sizes of dust deposited at Mfabeni during the LGM suggests that an increase in aridity was accompanied by a concomitant intensification in atmospheric circulation. In Maputaland, storm systems advancing northeast along the coast often generate gale force winds, which Orme (1973) regarded as the primary force driving coastal dune development. Enhanced aeolian activities and simultaneous dune development suggest that westerly storm tracks dominated the wind climate during this time. We propose that the northward migration of the westerly winds, which brought cool and drier conditions to the eastern region of southern Africa during the LGM, was accompanied by an increase in storminess and a strengthening in wind climate. An increase in wind intensity during this period was responsible for mobilising quartz-rich material enriched in heavy minerals from the local dunes, with an increase in local sand flux reflecting changes in the intensity of the westerly wind system. We compare our data to the only other available record of wind activity from the region covering the LGM, a reconstruction based on grain size from the SE Atlantic Ocean (Stuut et al., 2002; Fig. 6C). The Mfabeni record is broadly consistent with inferred increases in wind intensity during the LGM, and demonstrates that the influence of enhanced atmospheric circulation associated with the northward displacement in the westerly wind belt extended over the summer rainfall

region of southern Africa.

5.2.2. Lateglacial (18–11.5 kcal yr BP)

The record from Mfabeni reveals a rapid decline in aeolian activity following the LGM. However, higher than modern day fluxes of $45 \pm 4.4\ g\ m^{-2}\ yr^{-1}$ between 18 and 14.5 kcal yr BP suggest that cool and dry conditions persisted after the LGM. This is consistent with alkenone-inferred sea surface temperature (SST) reconstructions from the Mozambique Channel (Fig. 6E; Bard et al., 1997) and Atlantic Ocean (Kirst et al., 1999), which indicate that deglacial warming around southern Africa started ~15 kcal yr BP. A quantitative temperature reconstruction from Mfabeni further indicates that deglacial warming at the coast commenced ~16 kcal yr BP (Chevalier and Chase, 2015). Coupling between a rapid increase in SST and an approximate three-fold decrease in aeolian activity after 15 kcal yr BP suggests that changes in SST and its effect on position of the westerlies in the Southern Ocean was the dominant climate driver in the region during this time, while a shift toward fine-grained dust supports a weakening in atmospheric circulation over eastern South Africa.

5.2.3. Holocene (last 11.5 kcal yr BP)

Inferred warmer and humid conditions at the start of the Holocene correspond to an extended phase of increased SST around southern Africa. Reduced aeolian activities at this time thus likely reflect a combination of increased precipitation coupled with greater vegetation cover, dune stabilisation and decrease in source area. We link this to further contraction of the westerly wind polar vortex, resulting in enhanced easterly flow over eastern South Africa. This interpretation is consistent with southern African temperature records, which generally show that interglacial temperatures were established by 11–10 kcal yr BP, with maximum warming reached during the Holocene Altithermal at 8–6 kcal yr BP (Truc et al., 2013). Forest growth and expansion is indicated by the Mfabeni pollen record (Finch and Hill, 2008), supporting warm and relatively moist conditions during the Holocene Altithermal.

Although there is some uncertainty regarding the exact timing, the Mfabeni record provides support for a mid-Holocene arid phase. Inferred drier and more variable conditions ~6–4 kcal yr BP are consistent with regional pollen records (Neumann et al., 2014; Norström et al., 2014), and correspond with the onset of similarly dry conditions in Australia (Marx et al., 2011) and southern Chile (Lamy et al., 2001), which have been linked to an expansion in Antarctic sea ice and northward shift of the westerly storm track. An increase in aeolian deposition ~2–0.9 kcal yr BP coincides with a period of significant strengthening in El Niño–Southern Oscillation (ENSO) activity across the Southern Hemisphere (Moy et al., 2002; Gagan et al., 2004; Macreadie et al., 2015). Warm phases are typically associated with drought and wind erosion in eastern South Africa and have been linked to desiccation events at Lake St Lucia (Humphries et al., 2016). We tentatively attribute increases in aeolian deposition observed during the late Holocene to increased climate variability and prolonged dry periods associated with ENSO. However, more detailed analyses covering the Holocene period are required in order to better constrain the timing and magnitude of these arid events.

6. Conclusions

Aeolian records from the Southern Hemisphere covering the last glacial stage are scarce. We know of no existing long-term records of aeolian deposition from the summer rainfall region of southern Africa and this study thus provides new insight into links between aeolian activity, regional wind patterns, and climatic variability over glacial-interglacial timescales. The Mfabeni record documents substantial variations in aeolian flux associated with changes in regional climate and wind patterns that reflect larger scale climate patterns. Substantially higher fluxes observed during the LGM are linked to a reduction in vegetation cover and increase in local source areas brought about by a clear shift to dry and cool conditions. An increase in modal grain size and higher Ti concentrations support a strengthening in wind intensity during this period. We associate increases in wind intensity with a northward displacement in the westerly wind zone in the Southern Ocean and enhanced atmospheric circulation. Coupling between a rapid increase in SST and an approximate three-fold decrease in aeolian activity after 15 kcal yr BP suggests that a southward shift in the position of the westerlies the dominant climate driver in the region during deglaciation. Grain size distributions, Ti concentrations, and $^{87}Sr/^{86}Sr$ evidence indicates a warming in regional climate and greater precipitation that supported dune stabilisation after 15 kcal yr BP, with aeolian fluxes remaining suppressed throughout the early Holocene under the influence of enhanced tropical easterly flow. Our data supports a mid-Holocene arid phase in southern African climate 6–4 kcal yr BP, largely consistent with other regional palaeoclimate records, as well as an increase in climate variability associated with a strengthening in ENSO over the late Holocene.

The aeolian record from Mfabeni contributes to current knowledge of atmospheric circulations patterns in the Southern Hemisphere and supplements the limited palaeoenvironmental data available for southern Africa. Results from this study encourage further work aimed at examining changes in atmospheric dust deposition rates in a region where dust supply is known to have influenced Southern Ocean productivity during glacial-interglacial cycles. The potential of many lacustrine and peatland archives from southern African has yet to be fully explored, but may hold promising aeolian records for understanding shifts in atmospheric circulation in a region where traditional palaeoclimate archives are scarce.

Acknowledgments

We thank Liandra Bertolli, Luke Bodmann, Anel Geer, Leigh Gordon, Caldin Higgs, Trevor Hill, Sbu Mfeka, Letitia Pillay and Kate Strachan for enthusiastically assisting in the field. The iSimangaliso Wetland Park Authority and Ezemvelo KZN Wildlife granted us permission to work at Mfabeni. Sarushen Pillay assisted with laboratory processing and Carl Frisby is thanked for his assistance in the trace element and Sr-isotope analyses. The study was supported by funding from the South African National Research Foundation (Grant 84431), a University of KwaZulu-Natal Competitive Research Grant, and the University of the Witwatersrand. We acknowledge the constructive reviews of Paul Hesse and an anonymous reviewer which aided in focusing and clarifying the paper.

Appendix A. Supplementary data

Supplementary data to this article can be found online at http://dx.doi.org/10.1016/j.gloplacha.2017.08.002.

References

Anderson, R.F., Ali, S., Bradtmiller, L.I., Nielsen, S.H.H., Fleisher, M.Q., Anderson, B.E., Burckle, L.H., 2009. Wind-driven upwelling in the southern ocean and the deglacial rise in atmospheric CO_2. Science 323, 1443–1448.

Baker, A., Routh, J., Blaauw, M., Roychoudhury, A.N., 2014. Geochemical records of palaeoenvironmental controls on peat forming processes in the Mfabeni peatland, KwaZulu Natal, South Africa, since the late Pleistocene. Palaeogeogr. Palaeoclimatol. Palaeoecol. 395, 95–106.

Bard, E., Rostek, F., Sonzogni, C., 1997. Interhemispheric synchrony of the last deglaciation inferred from alkenone palaeothermometry. Nature 385, 707–710.

Björck, S., Clemmensen, L.B., 2004. Aeolian sediment in raised bog deposits, Halland, SW Sweden: a new proxy record of Holocene winter storminess variation in southern Scandinavia? The Holocene 14, 677–688.

Blaauw, M., Christen, J.A., 2011. Flexible paleoclimate age-depth models using an autoregressive gamma process. Bayesian Anal. 6, 457–474.

Chase, B.M., Meadows, M.E., 2007. Late quaternary dynamics of southern Africa's winter rainfall zone. Earth Sci. Rev. 84, 103–138.

Chase, B.M., Boom, A., Carr, A.S., 2013. Holocene climate change in southernmost South Africa: rock hyrax middens record shifts in the southern westerlies. Quat. Sci. Rev.

82, 199–205.
Chase, B.M., Lim, S., Chevalier, M., Boom, A., Carr, A.S., Meadows, M.E., Reimer, P.J., 2015. Influence of tropical easterlies in southern Africa's winter rainfall zone during the Holocene. Quat. Sci. Rev. 107, 138–148.
Chevalier, M., Chase, B.M., 2015. Southeast African records reveal a coherent shift from high- to low-latitude forcing mechanisms along the east African margin across last glacialeinterglacial transition. Quat. Sci. Rev. 125, 117–130.
Das, R., Bizimis, M., Wilson, A.M., 2013. Tracing mercury seawater vs. atmospheric inputs in a pristine SE USA salt marsh system: mercury isotope evidence. Chem. Geol. 336, 50–61.
De Jong, R., Björck, S., Björkman, L., Clemmensen, L.B., 2006. Storminess variation during the last 6500 years as reconstructed from an ombrotrophic peat bog in Halland, southwest Sweden. J. Quat. Sci. 21, 905–919.
Ellery, W.N., Grenfell, S.E., Grenfell, M.C., Humphries, M.S., Barnes, K., Dahlberg, A., Kindness, A., 2012. Peat formation in the context of the development of the Mkuze floodplain on the coastal plain of Maputaland, South Africa. Geomorphology 141–142, 11–20.
Finch, J.M., Hill, T.R., 2008. A late quaternary pollen sequence from Mfabeni Peatland, South Africa: reconstructing forest history in Maputaland. Quat. Res. 70, 442–450.
Gagan, M.K., Hendy, E.J., Haberle, S.G., Hantoro, W.S., 2004. Post-glacial evolution of the Indo-Pacific warm pool and El Niño-southern oscillation. Quat. Int. 118-119, 127–143.
Grundling, P., Baartman, L., Mazus, H., Blackmore, A., 2000. Peat Resources of KwaZulu-Natal Wetlands: Southern Maputaland and the North and South Coast. Council for Geoscience, Pretoria (Internal Report no. 2000–0132).
Grundling, P., Grootjans, A.P., Price, J.S., Ellery, W.N., 2013. Development and persistence of an African mire: how the oldest South African fen has survived in a marginal climate. Catena 110, 176–183.
Hesse, P.P., McTainsh, G.H., 1999. Last glacial maximum to early Holocene wind strength in the mid-latitudes of the southern hemisphere from aeolian dust in the Tasman Sea. Quat. Res. 52, 343–349.
Hogg, A.G., Hua, Q., Blackwell, P.G., Niu, M., Buck, C.E., Guilderson, T.P., Heaton, T.J., Palmer, J.G., Reimer, P.J., Reimer, R.W., Turney, C.S.M., Zimmerman, S.R.H., 2013. SHCal13 southern hemisphere calibration, 0–50,000 years cal BP. Radiocarbon 55, 1889–1903.
Holmgren, K., Lee-Thorp, J.A., Cooper, G.R.J., Lundblad, K., Partridge, T.C., Scott, L., Sithaldeen, R., Talma, A.S., Tyson, P.D., 2003. Persistent millennial-scale climatic variability over the past 25,000 years in Southern Africa. Quat. Sci. Rev. 22, 2311–2326.
Hua, Q., Barbetti, M., Rakowski, A.Z., 2013. Atmospheric radiocarbon for the period 1950–2010. Radiocarbon 55, 2059–2072.
Humphries, M.S., Green, A.N., Finch, J.M., 2016. Evidence of El Niño driven desiccation cycles in a shallow estuarine lake: the evolution and fate of Africa's largest estuarine system, Lake St Lucia. Glob. Planet. Chang. 147, 97–105.
Kirst, G.J., Schneider, R.R., Muller, P.J., von Storch, I., Wefer, G., 1999. Late quaternary temperature variability in the Benguela current system derived from alkenones. Quat. Res. 52, 92–103.
Kohfeld, K.E., Graham, R.M., de Boer, A.M., Sime, L.C., Wolff, E.W., Le Quere, C., Bopp, L., 2013. Southern hemisphere westerly wind changes during the last glacial maximum: paleo-data synthesis. Quat. Sci. Rev. 68, 76–95.
Lambert, F., Bigler, M., Steffensen, J.P., Hutterli, M., Fischer, H., 2012. Centennial mineral dust variability in high-resolution ice core data from Dome C, Antarctica. Clim. Past 8, 609–623.
Lamy, F., Hebbeln, D., Röhl, U., Wefer, G., 2001. Holocene rainfall variability in southern Chile a marine record of latitudinal shifts of the southern Westerlies. Earth Planet. Sci. Lett. 185, 369–382.
Lamy, F., Kilian, R., Arz, H.W., Francios, J.-P., Kaiser, J., Prange, M., Steinke, T., 2010. Holocene changes in the position and intensity of the southern westerly wind belt. Nat. Geosci. 3, 695–699.
Macreadie, P.I., Rolph, T.C., Boyd, R., Schröder-Adams, C.J., Skilbeck, C.G., 2015. Do ENSO and coastal development enhance coastal burial of terrestrial carbon? PLoS One 10 (12), e0145136.
Mahowald, N., Kohfeld, K., Hansson, M., Balkanski, Y., Harrison, S.P., Prentice, I.C., Schulz, M., Rodhe, H., 1999. Dust sources and deposition during the last glacial maximum and current climate: a comparison of model results with paleodata from ice cores and marine sediments. J. Geophys. Res. 104, 15895–15916.
Marx, S.K., Kamber, B.S., McGowan, H.A., Denholm, J., 2011. Holocene dust deposition rates in Australia's Murray-Darling Basin record the interplay between aridity and the position of the mid-latitude westerlies. Quat. Sci. Rev. 30, 3290–3305.
Moy, C.M., Seltzer, G.O., Rodbell, D.T., Anderson, D.M., 2002. Variability of El Nino/southern oscillation activity at millennial timescales during the Holocene epoch. Nature 420, 162–165.
Neumann, F.H., Botha, G.A., Scott, L., 2014. 18,000 years of grassland evolution in the summer rainfall region of South Africa: evidence from Mahwaqa Mountain, KwaZulu-Natal. Veg. Hist. Archaeobotany 23, 665–681.
Norström, E., Neumann, F.H., Scott, L., Smittenberg, R.H., Holmstrand, H., Lundqvist, S., Snowball, I., Sundqvist, H.S., Risberg, J., Bamford, M., 2014. Late quaternary vegetation dynamics and hydro-climate in the Drakensberg, South Africa. Quat. Sci. Rev. 105, 48–65.
Orme, A.R., 1973. Barrier and lagoon systems along the Zululand coast, South Africa. In: Coates, D.R. (Ed.), Coastal Geomorphology. New York State University, pp. 181–217.
Orme, L., Reinhardt, L., Jones, R.J., Charman, D.J., Barkwith, A., Ellis, M.A., 2016. Aeolian sediment reconstructions from the Scottish Outer Hebrides: late Holocene storminess and the role of the North Atlantic Oscillation. Quat. Sci. Rev. 132, 15–25.
Porat, N., Botha, G., 2008. The luminescence chronology of dune development on the Maputaland coastal plain, southeast Africa. Quat. Sci. Rev. 27, 1024–1046.
Ramsay, P.J., Cooper, J.A.G., 2002. Late Quaternary sea-level change in South Africa. Quat. Res. 57, 82–90.
Stager, J.C., Mayewski, P.A., Whitel, J., Chase, B.M., Neumann, F.H., Meadows, M.E., King, C.D., Dixon, D.A., 2012. Precipitation variability in the winter rainfall zone of South Africa during the last 1400 yr linked to the austral westerlies. Clim. Past 8, 877–887.
Stuut, J.-B.W., Prins, M.A., Schneider, R.R., Weltje, G.J., Jansen, J.H., Postma, G., 2002. A 300-kyr record of aridity and wind strength in southwestern Africa: inferences from grain-size distributions of sediments on Walvis Ridge, SE Atlantic. Mar. Geol. 180, 221–233.
Toggweiler, J.R., Russel, J.L., Carson, S.R., 2006. Midlatitude westerlies, atmospheric CO_2, and climate change during the ice ages. Paleoceanography 21. http://dx.doi.org/10.1029/2005PA001154.
Troels-Smith, J., 1955. Karakterisering af lose jordarter (Characterization of unconsolidated sediments). IV. Danmarks Geologiske Undersoegelsepp. 1–73.
Truc, L., Chevalier, M., Favier, C., Cheddadi, R., Meadows, M.E., Scott, L., Carr, A.S., Smith, G.F., Chase, B.M., 2013. Quantification of climate change for the last 20,000 years from Wonderkrater, South Africa: implications for the long-term dynamics of the intertropical convergence zone. Palaeogeogr. Palaeoclimatol. Palaeoecol. 386, 575–587.
Tyson, P.D., 1999. Atmospheric circulation changes and palaeoclimate of southern Africa. S. Afr. J. Sci. 95, 194–201.
Venter, C.E., 2003. The Vegetation Ecology of Mfabeni Peat Swamp, St Lucia, KwaZulu-Natal. (Unpublished MSc Thesis) University of Pretoria.
Wedepohl, K.H., 1995. The composition of the continental crust. Geochim. Cosmochim. Acta 59, 1217–1232.